Form and flow of the Devon Island Ice Cap, Canadian Arctic

J. A. Dowdeswell, T. J. Benham, and M. R. Gorman
Scott Polar Research Institute, University of Cambridge, Cambridge, UK

D. Burgess and M. J. Sharp
Department of Earth and Atmospheric Sciences, University of Alberta, Edmonton, Alberta, Canada

Received 15 September 2003; revised 15 January 2004; accepted 29 January 2004; published 10 April 2004.

[1] In this study, 3370 km of 100 MHz ice-penetrating radar data were acquired from Devon Ice Cap, Arctic Canada. Bed returns were obtained from >90% of flight tracks. Mean crossing point errors in ice surface elevation and ice thickness were 7–8 m. Digital elevation models of ice cap surface and bed elevation, and ice thickness, were produced and can be used as boundary conditions in numerical modeling. Devon Ice Cap, including 1960 km^2 of contiguous stagnant ice to its west, is 14,010 km^2. The ice cap proper is 12,050 km^2. Its largest drainage basin is 2630 km^2. The ice cap crest has a maximum measured elevation of 1921 m. Maximum recorded ice thickness is 880 m. Ice cap volume is 3980 km^3 (about 10 mm sea level equivalent). The bed, 8% of which lies below sea level, is an upland plateau dissected by steep-sided valleys that control the locations of the major outlet glaciers which dominate ice cap drainage. About 73 km, 4%, of the ice cap margin ends in tidewater. The margin is not floating. Icebergs of <100 m were observed offshore. Only a single outlet glacier showed signs of past surge activity. All major outlet glaciers along the eastern ice cap margin have retreated 1–3 km since 1960. Synthetic aperture radar-interferometic velocity structure shows slow, undifferentiated flow predominating in the west and center, with fast-flowing outlet glaciers and intervening slow-flowing ridges typical elsewhere. Outlet glacier velocities are 7–10 times higher than in areas of undifferentiated flow. This velocity structure, of fast-flowing units within slower-flowing ice, appears typical of many large (10^3 km^2) Arctic ice caps. *INDEX TERMS:* 1827 Hydrology: Glaciology (1863); 1824 Hydrology: Geomorphology (1625); 6969 Radio Science: Remote sensing; 9315 Information Related to Geographic Region: Arctic region; *KEYWORDS:* glaciology, radio-echo sounding, Arctic

Citation: Dowdeswell, J. A., T. J. Benham, M. R. Gorman, D. Burgess, and M. J. Sharp (2004), Form and flow of the Devon Island Ice Cap, Canadian Arctic, *J. Geophys. Res.*, *109*, F02002, doi:10.1029/2003JF000095.

1. Introduction

[2] The ice caps and glaciers of the Arctic islands make up about 45% of the 540,000 km^2 or so of ice outside Antarctica and Greenland, forming a significant area and volume fraction of the world's ice [*Dyurgerov and Meier*, 1997a, 1997b; *Dowdeswell et al.*, 1997; *Dowdeswell and Hagen*, 2004; *Dowdeswell*, 1995]. Over 151,000 km^2 of this ice is located in the Canadian Arctic islands [*Andrews*, 2002; *Koerner*, 2002]. The distribution of these ice masses within the Canadian Arctic archipelago is a function of the regional climate and climate gradients, together with the large-scale topography of the area. Major ice caps are present on the mountainous eastern sides of Ellesmere, Devon, and Baffin Islands (Figure 1), associated with a predominant moisture source from the southeast [*Koerner*, 1979]. The largest ice caps in the Canadian Arctic, and indeed in the Arctic as a whole, include the Devon Ice Cap (~14,000 km^2) on Devon Island and the Agassiz Ice Cap (~17,300 km^2) on Ellesmere Island (Figure 1).

[3] Deep ice cores, collected from ice caps on Devon, Ellesmere, and Baffin Islands, have been used to reconstruct the climate history of the eastern Canadian Arctic [e.g., *Koerner*, 1977a, 1997; *Koerner and Fisher*, 1990; *Fisher et al.*, 1998], and the mass balance of a number of glaciers and ice caps has been investigated systematically over the past 40 years or so [e.g., *Koerner*, 2002]. However, numerical modeling of Canadian Arctic ice caps, and thus predictions of their likely responses to future and past climate changes, has been largely precluded because very little information is available on their three-dimensional morphology; this applies particularly to model boundary conditions of ice thickness and the topography of the underlying bedrock [cf. *Koerner*, 1977b].

[4] In this paper we present detailed observations of the form and flow of the Devon Ice Cap (Figure 1), derived mainly from airborne 100 MHz ice-penetrating radar survey and ancillary satellite data. This ice cap was selected for investigation because of the existence of evidence on its

0148-0227/04/2003JF000095$09.00

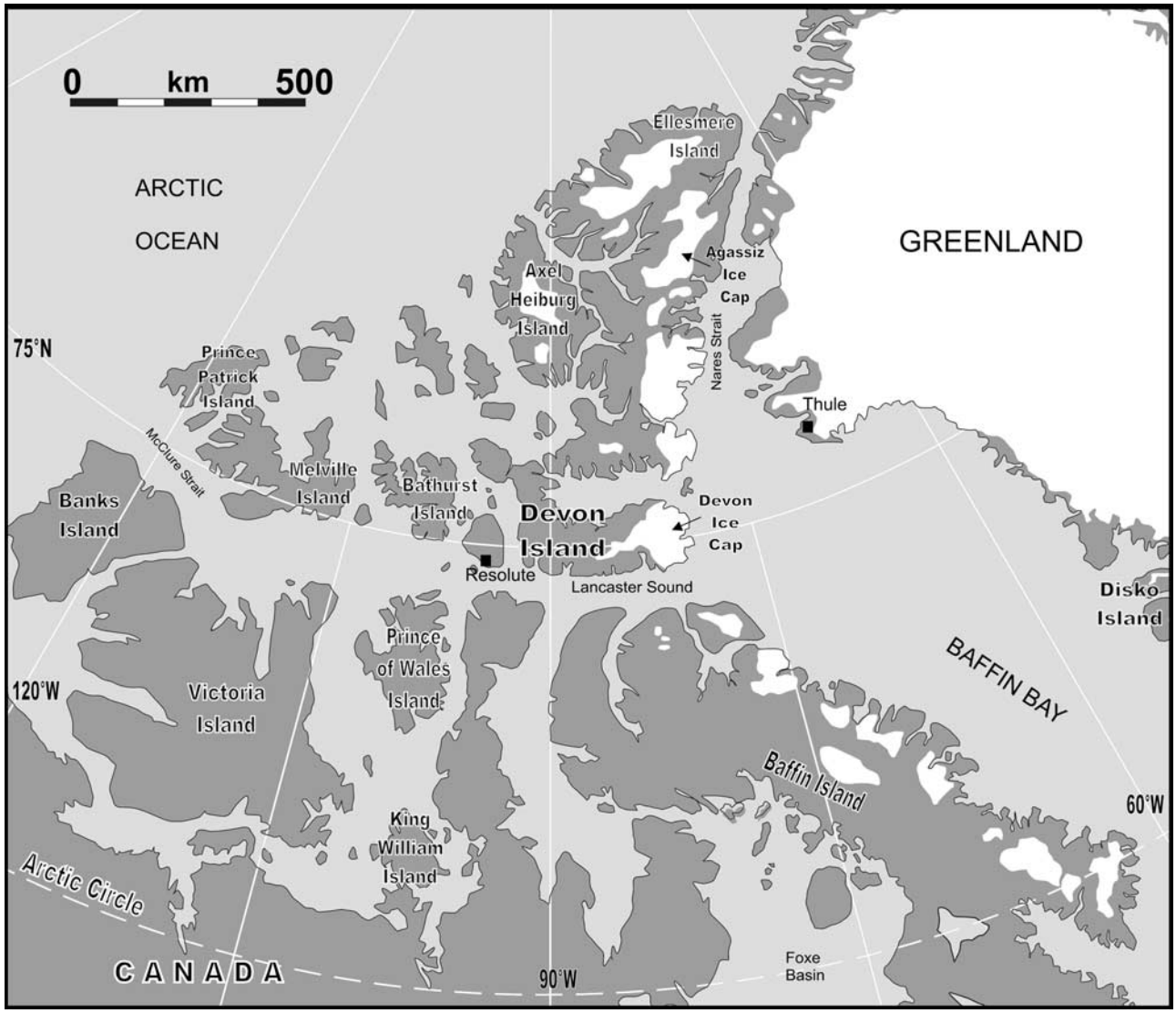

Figure 1. Map of the Canadian Arctic islands, with the Devon Ice Cap and other ice masses in northern Canada and Greenland shown in white.

climate and mass balance history [e.g., *Koerner*, 1977a, 2002] and because of its relatively large size but simple surface form. In a broader environmental context, general circulation models (GCMs) predict that the Arctic will warm preferentially over the next hundred years or so relative to lower latitudes, thus making the changing form and flow of Arctic glaciers and ice caps important to future projections of global sea level in a warming world [e.g., *Cattle and Crossley*, 1995].

2. Methods

2.1. Airborne Radar Investigations

[5] Our airborne radar studies of the ice thickness of the Devon Ice Cap used a 100 MHz system. The radar instrument was the same as that fabricated by M. R. Gorman and used previously in our radar investigations of the ice caps on Russian Severnaya Zemlya [*Dowdeswell et al.*, 2002]. The specifications of the radar system are given in Table 1. The antennae were two half-wave dipoles mounted beneath the aircraft wings, with one for transmitting and the second for receiving. Antenna gain was 8 dB (one way). A digital data acquisition system recorded data, employing a fast digitizer to record complete waveforms, allowing the recovery of absolute power levels and power reflection coefficients. An example of a digital radar record across the Devon Ice Cap is given in Figure 2.

[6] The program of airborne radio echo sounding on the Devon Ice Cap took place between 4 April and 14 April 2000. Data acquisition well before the beginning of the melt season insured that there was no increase in signal absorption associated with summer meltwater in the snowpack [*Smith and Evans*, 1972]. Scientific flying was undertaken from a de Havilland Twin Otter fixed-wing aircraft, operated from Resolute Bay on Cornwallis Island with refueling at Grise Fjord on Ellesmere Island during some missions (Figure 1). The flights were at a nominal air speed of $\sim$230 km hr^{-1} and were flown at a constant pressure altitude, which ranged from 700 to 1100 m, depending on weather conditions. A series of seven scientific flights of up

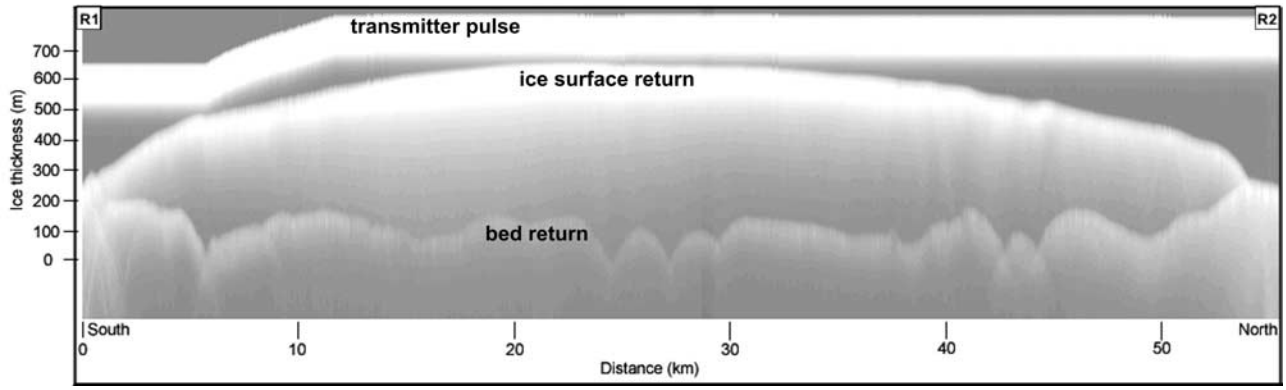

Figure 2. Example of 100 MHz ice-penetrating radar data obtained from the Devon Ice Cap. The *y* axis has been converted from time delay into ice thickness using a radio wave velocity in ice of 168 m μs^{-1}. The flight line (R1–R2) is located in Figure 3.

to 3 hours duration was undertaken. On each flight a significant amount of time was required for positioning legs over land or water. Dedicated flights were also made for equipment testing after installation and for over-water calibration of the radio echo sounding system. To locate the aircraft position and altitude, GPS positions and pressure altimeter data were recorded.

[7] GPS records of aircraft position were collected and differentially postcorrected using data from base stations at Resolute (74°43′N, 94°59′W), Thule (76°32′N, 68°47′W), and on the Devon Ice Cap itself (75°21′N, 82°08′W) (Figure 1). Differential correction accuracy degrades as the distance between the aircraft and base stations increases. Distances from the Resolute and Thule base stations to the nearest and furthest margins of the Devon Ice Cap are 290–455 km and 315–465 km, respectively. Average errors in navigation are ~5 m for horizontal positions and ~9 m in the vertical at a 95% level of confidence.

[8] A map of the flight lines over the Devon Ice Cap is given in Figure 3. The ice cap was covered by a nominal 10 km spaced grid of flight lines. Several additional lines were also acquired from flow lines down specific outlet glaciers that were unsuitable for coverage by the gridding scheme. A total of 3370 km of radar data were obtained over the Devon Ice Cap.

[9] The digital radar data were analyzed by plotting waveforms in Z-scope mode, in raw data number, differentiated, or start-of-rise-point form. Reference was made to individual A-scope waveforms where necessary. Tracking algorithms for delineating horizons for first surface and bed returns need to locate the start of sustained rises in returned power levels and to identify continuity of the tracked horizon in subsequent waveforms [*Cooper*, 1987]. While automated tracking of interfaces had some success on relatively smooth horizons, loss of lock meant that the algorithm needed restarting frequently. We found that the optimal means of tracking interfaces was in a semimanual fashion, with the operator tracing along the approximate location of an interface on a Z-scope display and the delineated points being "snapped" to the nearest start of power rise. For suppression of noise in individual waveforms we typically averaged five waveforms (~7 m in along-track distance), although in areas of noisier data, it was possible to average greater numbers of waveforms to better identify reflectors. The interfaces thus tracked could be overlain on the raw mode Z-scope display for assessment. In areas where there was potential for misidentification of interfaces due to off-nadir echoes from subaerial valley walls, Landsat Enhanced Thematic Mapper Plus (ETM+) imagery was overlain by flight position and interface-tracking information to assist identification of echo sources [*Benham and Dowdeswell*, 2003].

[10] Differentially corrected GPS records provided absolute aircraft altitudes. Aircraft pressure-altimeter measurements were also calibrated over the sea surface adjacent to the ice cap. Where three-dimensional GPS positions were either absent or unreliable, pressure-derived altitude data were used. Ice surface elevations were then derived by subtracting aircraft terrain clearance measured by the radar from the absolute altitude of the aircraft.

[11] Analysis of the differences in measured ice surface elevation and ice thickness at points where flight tracks crossed was used to assess random errors in our measurements. The distribution of these errors was not constant over the ice cap. Larger errors in ice surface elevation were generally distributed around areas of steeper slope or more complicated topography, such as at the steeper margins of the ice cap. The mean difference in ice surface elevation measurements at crossing points was 7.7 m, with 155 of the 165 crossing points located within 20 m of one another.

[12] The largest crossing point errors in the measurements of ice thickness were generally in areas of more complicated bedrock and/or surface topography. Some of these were concentrated in areas of thicker ice southeast of the center of

Table 1. System Parameters of the 100 MHz Radar Used in the Canadian Arctic

Parameter	Value
Center frequency, MHz	100
Transmitter pulse length, μs	0.35 or 1.1
Transmitter peak pulse power, W	250 or 1000
Transmitter pulse rate, kHz	10
Receiver bandwidth, MHz	30 or 3
Receiver type	successive detection log amplifier
Receiver noise, dB	6
System performance (excluding antenna gain), dB	
Short pulse	150
Long pulse	160

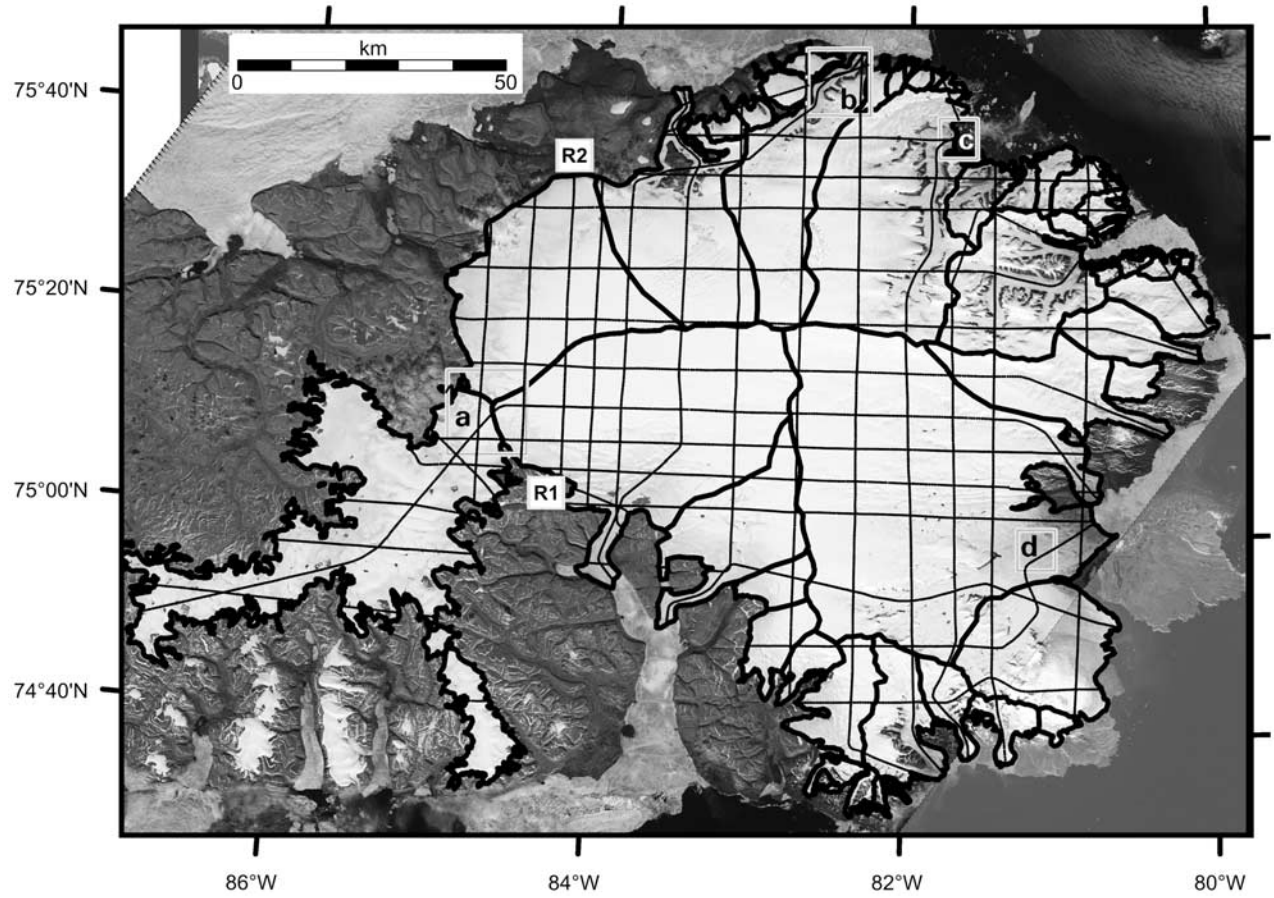

Figure 3. Landsat Enhanced Thematic Mapper Plus (ETM+) image mozaic of the Devon Ice Cap, showing the boundaries of major ice cap drainage basins (thick black lines) and the grid of flight lines from which airborne radio echo sounding data was obtained (thin black lines). The radar transect shown in Figure 2 (R1–R2) is located. The boxes labeled a–d locate the four subscenes making up Figure 4.

the ice cap, where radio echo returns from the ice cap bed were weakest due to greater absorption of electromagnetic energy along a longer two-way path length and to scattering by ice inclusions within firn of the accumulation zone. The mean crossing point error in ice thickness measurements was 7.5 m, with 111 of 116 crossing points located within 20 m.

[13] Our reduced radar measurements of ice surface elevation and ice thickness along flight lines were then interpolated over the whole ice cap to produce digital elevation models (DEMs) for use in, for example, numerical modeling of the Devon Ice Cap. For modeling purposes the DEM grid cell size used should be greater than the ice thickness. Given a maximum observed ice thickness of ~900 m, a cell size of 1 km was selected. In line with the practice of the Antarctic BEDMAP project [*Lythe et al.*, 2001], we extracted data at regular intervals along track from each flight line. While the ice surface elevation, as a property that tends to vary smoothly, could be characterized adequately by sampling at regular intervals, the ice thickness and bedrock data exhibited more high-frequency variability. We therefore added a number of additional ''points of interest'' from visual inspection of Z-scope profiles and included these as data points.

[14] For interpolation of our reduced radar measurements of ice surface elevation and ice thickness over the whole ice cap we had envisaged using ordinary kriging with prior semivariogram analysis [*Isaaks and Srivastava*, 1989]. Kriging is an optimal interpolator of irregularly spaced point data. However, we were not able to apply this technique to our satisfaction for the Devon Ice Cap. No single semivariogram model fitted the data adequately, and trial interpolations carried out using kriging and other methods such as splining did not yield results that were consistent with the input point data. Given that the intention was to generate DEMs which characterize the average elevation or thickness in 1 km cells, an inverse distance weighting (IDW) method was chosen.

[15] To address artifacts from the directional effects of the radar survey pattern (Figure 3), we implemented, in line with the BEDMAP approach [*Lythe et al.*, 2001], our own IDW interpolation algorithm using an eight-point directional search for input data points. This method was generally successful in removing the bias toward data points from the nearest flight line, and the use of a block-smoothing approach further reduced such effects. However, for the surface elevation DEM we encountered artifacts in maximum slope calculations which we believed to result from the additional smoothing used. We therefore generated surface elevation DEM values using the ArcInfo TOPOGRIDTOOL facility [*Hutchinson*, 1993]. This uses a

locally adaptive splining model which enforces hydrological rules. Bed elevation DEM values used in final products were derived from ice surface elevation minus ice thickness values for the same grid cell. This is in keeping with the fact that ice thickness is the primary parameter extracted from radio echo sounding data and that bed elevation is a derived quantity. For the purposes of numerical modeling, grid cells were also defined for 5 km beyond the present ice cap margin from our radar data, allowing ice advance as well as retreat to be reconstructed effectively during modeling work.

[16] It is clear from Landsat ETM+ imagery of the Devon Ice Cap that outlet glaciers constrained within rock walls are an important component of ice cap form and flow (Figure 3). Ignoring such boundaries to flow resulted in ice thickness and bedrock elevation interpolation artifacts. Using Landsat imagery as a backdrop within a geographic information system (GIS), a polygon coverage of rock wall boundaries to ice flow was produced. This was then used to restrict the choice of input points for our interpolation to those relevant to the channelized ice flow and prevented such important topographic features from being removed or subdued in the interpolation.

2.2. Satellite Remote Sensing

2.2.1. Landsat Imagery

[17] Landsat ETM+ digital imagery (Figure 3), with a spatial resolution of 15 m in panchromatic mode [*Bindschadler et al.*, 2001], was used for several purposes during our investigations of the Devon Ice Cap. First, Landsat imagery was used to map the margins of the ice cap after georeferencing to ground control points. Secondly, the qualitative topography of the ice cap surface, including the location of ice divides defining ice cap drainage basins, was derived from digitally enhanced Landsat pixel brightness values [e.g., *Martin and Sanderson*, 1980; *Dowdeswell et al.*, 1995]. This surface topographic information was used in the planning of aircraft flight lines for radio echo sounding.

[18] Landsat imagery and aerial photography from 1959/1960 were examined for the presence of indicators of surge behavior on both Devon Ice Cap and also, more generally, over the ice masses of Ellesmere and Axel Heiberg Islands [*Copland et al.*, 2003]. A number of ice surface features have been used as indicators of whether or not glaciers and larger ice masses have undergone periodic surge behavior during the residence time of the ice within a given drainage basin. These features include [*Meier and Post*, 1969] (1) looped medial moraines, formed as fast-flowing, active-phase surge-type glaciers flow past less active or stagnant neighbors and deform the medial moraines between them and preserved over the residence time of ice within the system; (2) potholes on the glacier surface during the quiescent phase; and (3) a heavily crevassed surface indicative of a glacier in the active phase of the surge cycle and often, although not always, associated with rapid terminus advance. These features can be recognized readily on Landsat imagery and aerial photography [e.g., *Dowdeswell and Williams*, 1997].

2.2.2. Synthetic Aperture Radar (SAR) Interferometry

[19] Few velocity measurements of the Devon Ice Cap have been made; *Doake et al.* [1976] measured a velocity of 2.4 m yr^{-1} near the ice cap crest using radar fading patterns, and *Cress and Wyness* [1961] recorded winter and summer velocities of 36 and 65 m yr^{-1}, respectively, ~5 km from the terminus of Sverdrup Glacier, an outlet draining the northwest side of the ice cap. Satellite radar interferometry provides a tool for measuring velocity structure synoptically across whole ice masses. The interferograms produced for the Devon Ice Cap are derived from pairs of ERS-1/2 synthetic aperture radar (SAR) images acquired during the 1996 tandem-mode mission over the southeast and western regions and from 1992 3 day repeat pass data over the northeast quadrant. The phase difference in an interferogram is a result of range change between two satellite passes, where range is affected by both horizontal and vertical ice displacement as well as by the interferometric baseline between passes. The effects of ice surface topography are removed by subtracting a synthetic interferogram generated from an external DEM [*Massonet et al.*, 1993] or by double differencing between two tandem-mode interferometric pairs [*Gabriel et al.*, 1989]. Errors in interferometric baseline estimates can also introduce a quasi-linear phase ramp of several fringes across an image [*Joughin et al.*, 1996]. This ramp has been removed through subpixel coregistration between the slave and master images together with tie points selected over areas of bare land [*Zebker et al.*, 1994], where displacement should be zero.

[20] Interferograms of the Devon Ice Cap were generated using the above methods and corrections. They can be viewed as contour maps of surface displacement in the satellite look direction, with each fringe (i.e., cycle of the color wheel) representing a change of 20 m yr^{-1}. The errors in the velocity estimates, which are dependent on the interferometric baseline and the accuracy of the external DEM, were 0.92, 1.26, and 2.7 m yr^{-1} for the southeast, west, and northeast sectors of the ice cap, respectively. Coherent interferometric fringes were produced over almost the whole ice cap. These data were phase unwrapped and then used to produce ice surface velocities in the look direction of the SAR. Look direction velocities, rather than those in the direction of ice flow, are presented in this study because they are well suited for identifying coherent flow units as well as subtle changes in ice motion over large areas.

3. Results: Ice Cap Morphology, Thickness, and Velocity Structure

3.1. Ice Surface Morphology

[21] The total area of the Devon Ice Cap is 14,010 km^2, measured digitally from Landsat ETM+ imagery. However, the ice-covered area extending westward from the main ice cap is a subsidiary ice body (Figure 3). This ice appears from Landsat imagery to be both dynamically separate from the main ice cap and also likely to be of very low surface gradient (Figure 4a). The entire margin of this subsidiary, 1960 km^2 ice body ends on land; it is referred to informally as the "western Devon Ice Cap" here. Subtracting this from the total ice-covered area yields an area of 12,050 km^2 for the Devon Ice Cap proper.

[22] The surface of the Devon Ice Cap is relatively simple and dome-like in shape. A DEM of the ice surface, derived from our airborne radar data, is shown in Figure 5. This ice

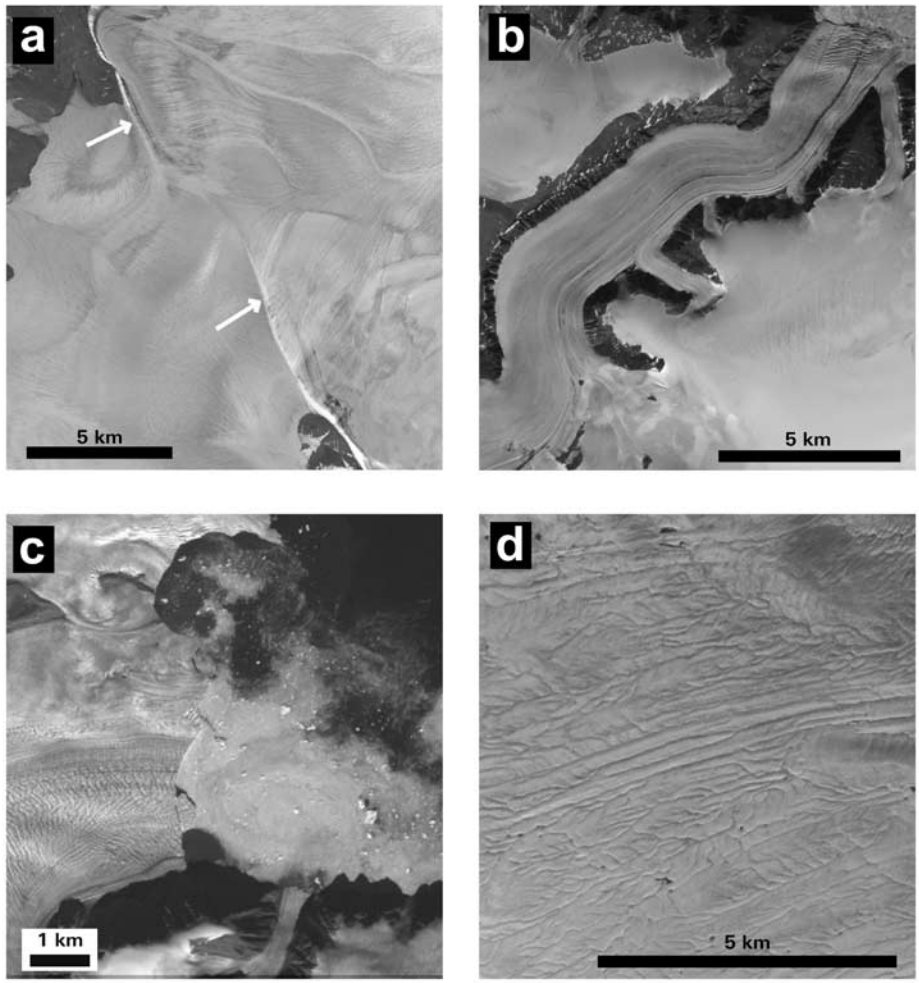

Figure 4. Landsat ETM+ images of parts of the ice cap on Devon Island. Each subscene is located in Figure 3. Glacier names are shown in Figure 8. (a) The well-defined boundary (marked with arrows) between the main Devon Ice Cap to the right and the thin and inactive "western Devon Ice Cap" to the left. (b) Eastern Glacier, an outlet glacier constrained by valley walls and ending in a crevassed tidewater margin. (c) The heavily crevassed tidewater terminus of Belcher Glacier, with several icebergs located within brash ice offshore. (d) A closely spaced network of supraglacial stream channels incised into the surface of the low-gradient lobe on the southeast of Devon Ice Cap. Note that some streams terminate at moulins, implying that supraglacial meltwater probably reaches the glacier bed.

surface DEM, together with those for ice thickness and bed elevation, are obtainable as auxiliary material to this paper[1]. The crest of the ice cap reaches a maximum measured elevation of 1921 m. Ice surface ridges run east, north, and south from the summit, with the eastward being the most pronounced. To the west, the ice cap surface has a very simple form, sloping down gently to terminate on land. Mountain ridges rise above the ice surface to the north and south of the crest in particular (Figure 3). The rock ridges form the walls of outlet glaciers that drain the central area of the ice cap. In addition, the area-altitude distribution, or hypsometry, of the ice cap is an important control on snow accumulation and surface melting and is a vital parameter in mass balance studies [*Hagen and Reeh*, 2004]. The distribution of ice cap surface elevation with altitude is illustrated in Figure 6a. The area-elevation curve is relatively smooth, with a minor peak at ~1000–1100 m above sea level.

[23] The Devon Ice Cap is drained by a number of outlet glaciers. Examples include Eastern and Belcher Glaciers (Figures 4b and 4c). These outlet glaciers are constrained by valley walls, with the ice-filled valleys probably being similar in configuration to the series of steep-walled canyons cut into bedrock that are typical of the terrain beyond the ice cap margin. Among the largest of these outlet glaciers, Belcher and Sverdrup Glaciers draining northward into Jones Sound and Cunningham Glacier flowing south into Lancaster Sound are 35, 25, and 20 km long, respectively. The southeastern region of the ice cap is rather different in surface form from the rest of the ice cap margins, being less well constrained by mountain topogra-

[1]Auxiliary material is available at ftp://ftp.agu.org/apend/jf/2003JF000095.

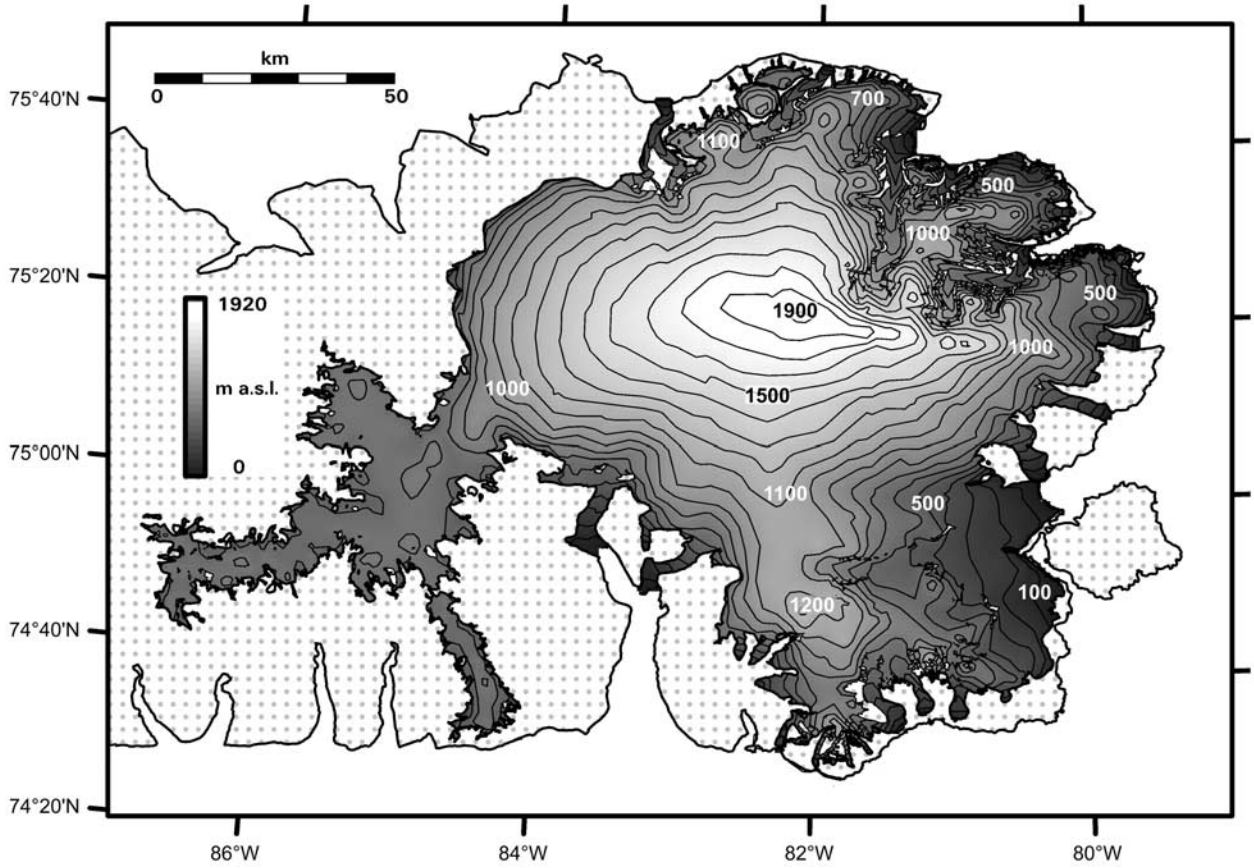

Figure 5. Ice surface elevation map of the Devon Ice Cap (contour interval 100 m).

phy; the marginal 15 km or so of the ice cap flows into marine waters at a gentle gradient here.

[24] The total length of tidewater ice cliffs at the margins of the Devon Ice Cap is 73 km. This makes up ~4% of the ice cap edge, with the remainder ending on land. Over 75% of these ice cliffs are the termini of outlet glaciers that are, individually, less than ~2.5 km in width. The longest section of ice cliffs, in the southeast of the ice cap, totals about 18 km in length. Icebergs are produced from the crevassed tidewater margins of the ice cap. The largest icebergs observed on Landsat imagery and during airborne radar work were <100 m in maximum diameter (Figure 4c). There is little evidence that these tidewater ice margins are floating in the form of either significant areas of very low ice surface slope or the production of large tabular icebergs. These criteria have been used previously to infer the presence of floating ice margins in Greenland and the Russian Arctic islands [*Higgins*, 1991; *Dowdeswell et al.*, 1994; *Williams and Dowdeswell*, 2001].

3.2. Ice Thickness and Bed Elevations

[25] The thickness of Devon Ice Cap, measured using our 100 MHz radar system, is illustrated as a DEM in Figure 7. The maximum recorded ice thickness is 880 m, slightly southeast of the center of the ice cap at 75°10′N, 81°18′W. From this DEM a volume of 3980 km^3 is calculated for the main Devon Ice Cap. The additional volume of the western Devon Ice Cap is a further 130 km^3. If the Devon Ice Cap were to melt completely, it would contribute ~10 mm to the global sea level.

[26] In general, ice thickness increases most rapidly close to the ice cap margin and then continues to increase more slowly and monotonically toward the central dome. The thickest ice, between ~700 and 880 m deep, is located to the northeast and southeast of the geographical center of the ice cap (Figure 7). An extensive area of thin ice, <350 m thick and covering ~400 km^2, occurs in the southeast of the ice cap. This piedmont area is fed by several outlet glaciers, which flow through the mountains to the west. The western Devon Ice Cap, by contrast, forms only a thin carapace of ice over bedrock (Figure 4a), with a maximum recorded thickness of 240 m.

[27] The absolute altitude of the bed of the Devon Ice Cap is presented as a DEM in Figure 8. The ice cap bed hypsometry is also shown in Figure 6b. The vast bulk of the bed of the main ice cap, and all of the smaller ice body to the west, lies above sea level. The bed appears to be an upland plateau, dissected by a series of steep-sided valleys (Figure 8). Mountain summits and ridges break the ice cap surface in the north and south; the Treuter and Cunningham Mountains are most prominent. The subglacial valleys and subaerial valley walls appear to control the locations of the major outlet glaciers draining the Devon Ice Cap. Subglacial valleys also influence the direction of ice flow into the southeastern piedmont lobe.

[28] Only 8% of the ice cap bed lies below present sea level (Figure 6b). This is confined to two types of areas: First, the marginal few kilometers of most outlet glaciers, including their tidewater termini, have beds below sea level;

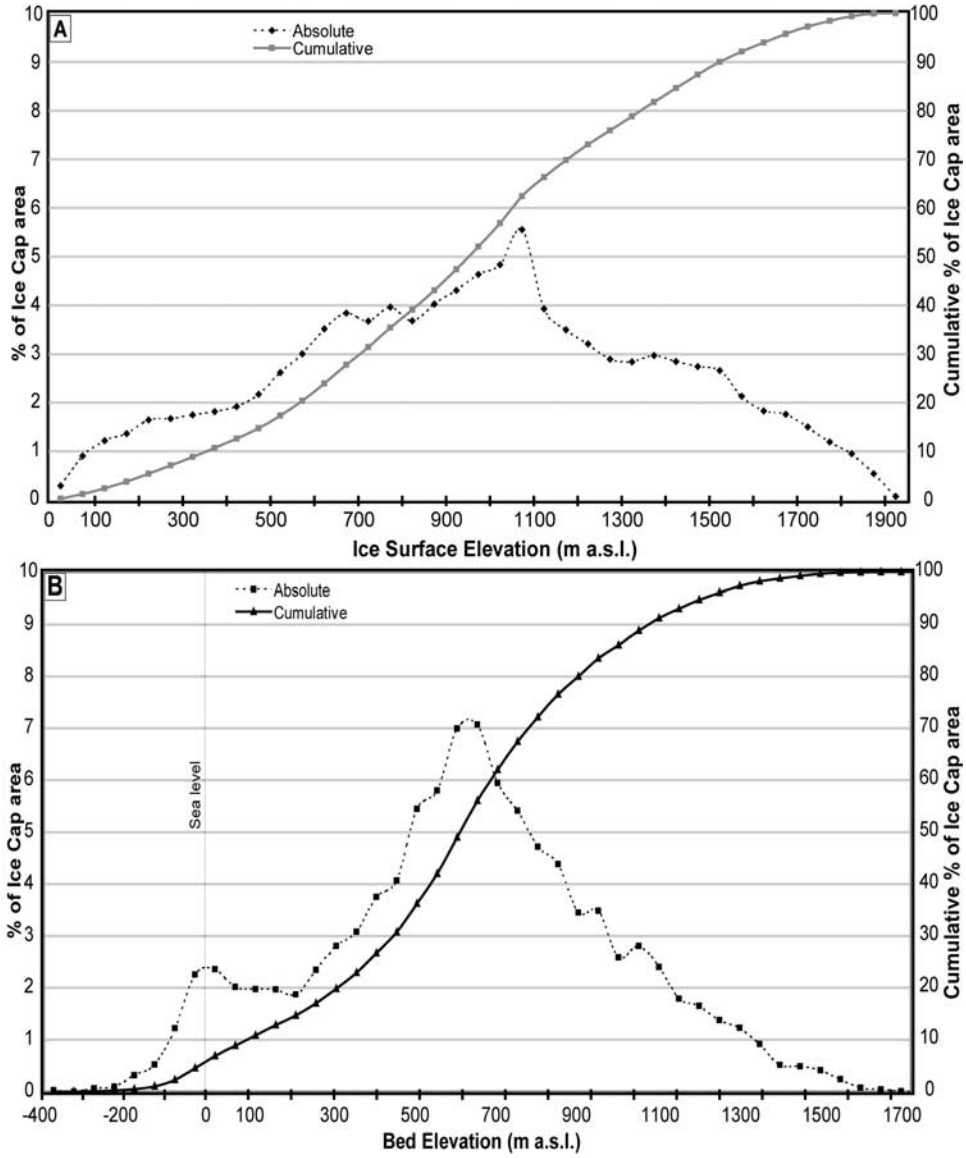

Figure 6. Hypsometry of the 12,050 km^2 Devon Ice Cap. (a) Ice surface elevation (m). (b) Subglacial bed elevation (m). Hypsometric curves are given for each elevation band and for the cumulative percentage. The 1960 km^2 western Devon Ice Cap is excluded.

secondly, the piedmont ice cover in the southeast of the ice cap is largely grounded below sea level (Figure 8). Several of the larger outlet glaciers, including Sverdrup and Belcher Glaciers draining northward and the two tidewater glaciers flowing south into Croker Bay, have beds lying several hundred meters below present sea level that extend between 15 and 20 km from the ice margin. It is likely that the bed in these areas is made up of glacier-influenced marine sediments, which would have accumulated at times over the late Quaternary when the Devon Ice Cap was smaller or disappeared, as environmental records from the deep ice core taken close to the ice cap summit and investigations of Holocene sedimentation in Bear Lake adjacent to the northwestern ice cap margin indicate [*Koerner*, 1977a; *Lamoureux et al.*, 2002].

[29] Radar returns from the bed of the Devon Ice Cap were acquired from ~91% of the flight tracks. The main areas where bed echoes were absent were in zones of intense surface crevassing, associated particularly with steep icefalls on outlet glaciers, or where bed returns were masked by significant valley sidewall echoes. Some loss of bed reflection may be a result of nonoptimal terrain clearance or aircraft attitude while repositioning with respect to terrain elevation change.

3.3. Velocity Structure From SAR Interferometry

[30] SAR interferometry was used to map the velocity structure of the Devon Ice Cap and, in particular, the extent and distribution of fast-flowing ice (Figure 9). The most notable pattern in the interferogram is the slow and undifferentiated velocities in the west and central region of the ice cap as compared with outlet glaciers and intervening slow-flowing ridges elsewhere (Figures 9 and 10). A number of fast-flowing units identified in SAR interferometry usually

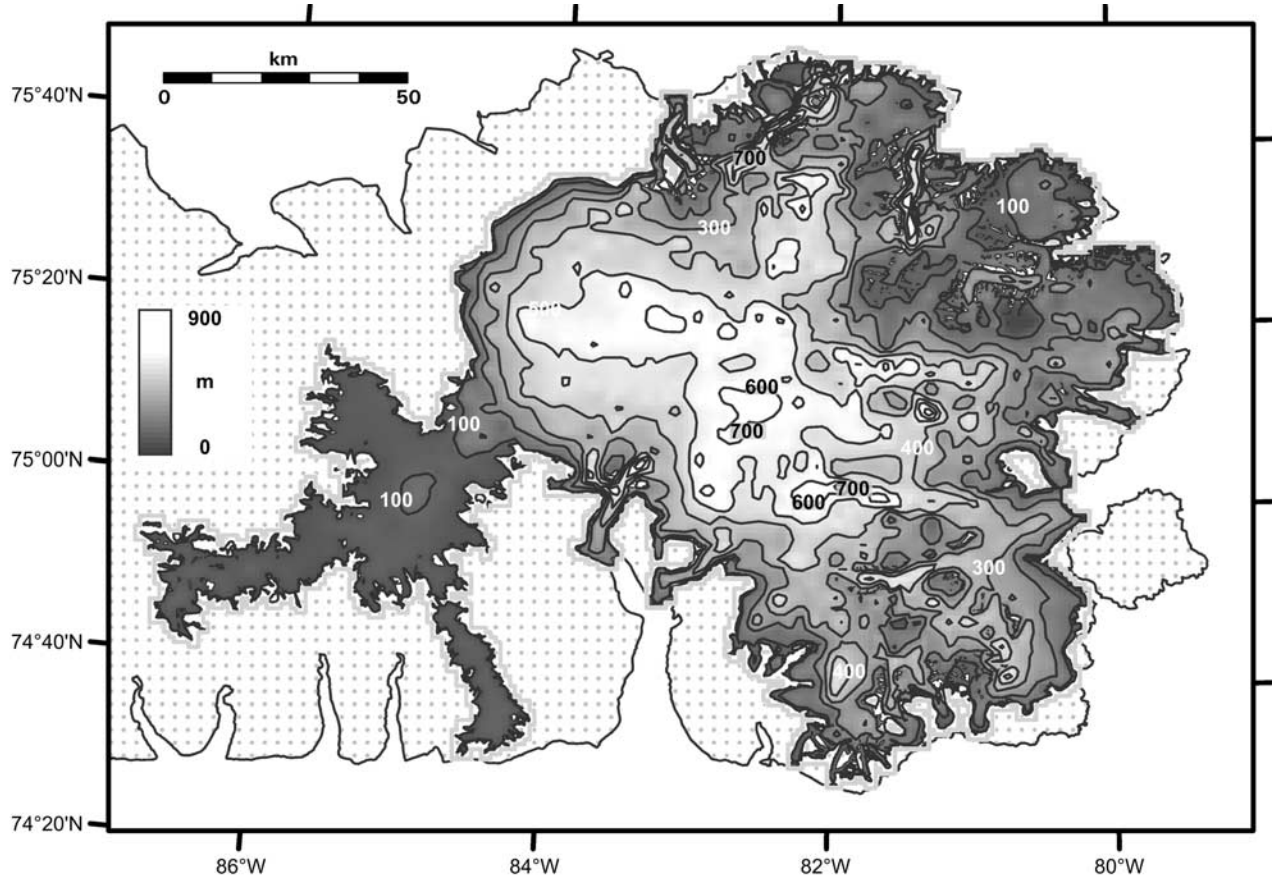

Figure 7. Ice thickness distribution on the Devon Ice Cap (contour interval 100 m).

occupy troughs in the bedrock topography over all or part of their length (Figures 10a and 10b). Surface velocities in these outlet glaciers of the ice cap are typically 7–10 times higher than in adjacent areas of undifferentiated flow.

4. Flow of the Devon Ice Cap

4.1. Inferences From Landsat Imagery

[31] Landsat ETM+ imagery of the Devon Ice Cap shows clearly that ice flow outward from the crest of the ice cap is mainly through outlet glaciers channeled within a series of bedrock-sided valleys (Figure 3). Most of these outlet glaciers end in tidewater (Figures 4b and 4c). Their margins are usually crevassed, with the crevasses generally oriented perpendicularly to ice flow, indicating longitudinal tension. This is typical of the stress regime found close to the unconstrained ice walls of tidewater glaciers [e.g., *Hodgkins and Dowdeswell*, 1994].

[32] Where mountainous terrain is absent (Figure 8), the ice cap surface appears largely smooth on Landsat imagery; the northwest sector of the ice cap is the best example of this form of simple radial flow (Figure 3). By contrast, the piedmont lobes on the southeast side of the ice cap have a very distinctive ice surface morphology developed on a surface of very low gradient. Dense networks of supraglacial stream channels appear almost ubiquitous on Landsat imagery in this area (Figure 4d). Many of these channel systems end abruptly, with meltwater presumably descending to the glacier bed via moulins.

[33] Landsat imagery was also used to examine the drainage basins and outlet glaciers of the Devon Ice Cap for indicators of present or past surge activity. *Copland et al.* [2003] reported that a single outlet glacier of the ice cap, the western branch of Cunningham Glacier (74°34′N, 81°25′W), exhibited extensive surface folding combined with a 2 km retreat between 1959 photographs and 1999 imagery, implying past surge activity. Other outlet glaciers of the ice cap showed no indicators of past surges [*Copland et al.*, 2003], according to the criteria of *Meier and Post* [1969]. However, all the major outlet glaciers along the eastern margin of the ice cap have experienced retreat ranging from 1 to 3 km since 1960 (D. Burgess and M. J. Sharp, personal communication, 2003). Given the lack of evidence of ice surface features indicative of past nonsteady flow, such retreat is more likely to be a response to climate change than to past surge activity.

[34] Finally, the major ice divides and drainage basins on the ice cap have been mapped using a combination of the Canadian Digital Elevation Dataset (CDED) DEM, Landsat imagery, SAR interferometry, and bedrock topography (Figure 3). Basins were originally delineated based on the surface topography represented by the CDED DEM using the hydrological modeling tools in ArcView GIS. Placement of the modeled basin boundaries was guided by interpretation of the surface topography evident in the 1999 Landsat 7 ETM+ orthomosaic. Drainage divides were refined further by comparing the drainage basin boundaries with the source regions of major outlet glaciers

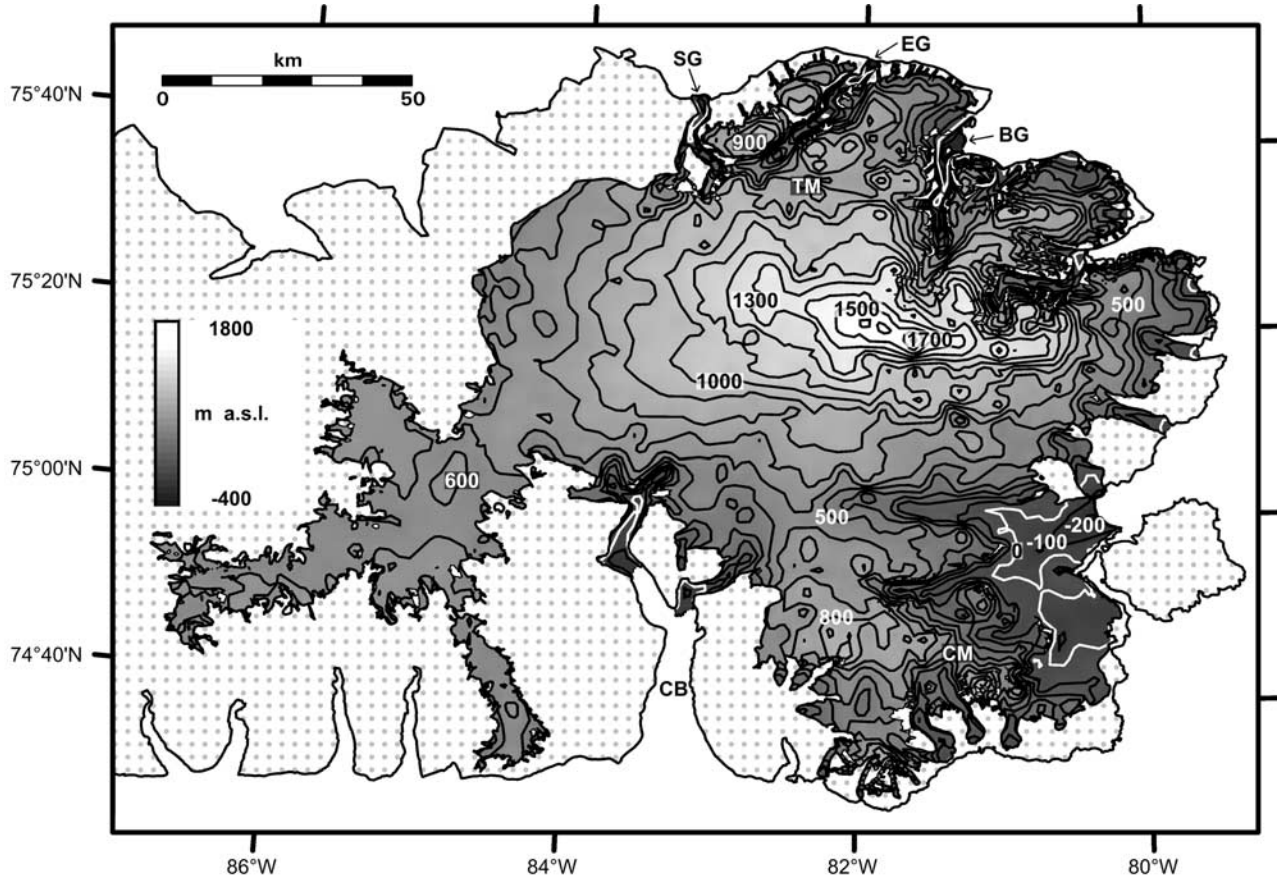

Figure 8. Bed elevation map of the Devon Ice Cap (contour interval 100 m). Note that the zero, or sea level, contour is white. SG, Sverdrup Glacier; EG, Eastern Glacier; BG, Belcher Glacier; CB, Croker Bay; CM, Cunningham Mountains; TM, Treuter Mountains.

and ice streams. Source regions were effectively highlighted by the pattern of accelerated ice flow in the SAR interferometry throughout the interior regions, where surface topography is subtle (Figure 9). Finally, the bedrock topography derived in this study was used to identify divides based on subglacial ridges (not evident at the surface) to mark the point of flow divergence throughout regions of uniform sheet flow. The largest drainage basin is 2630 km^2 in area and is drained primarily by the two large outlet glaciers in the southeast sector of the ice cap (Figure 3).

4.2. Pattern of Ice Flow

[35] The velocity pattern derived from SAR interferometric analysis of the Devon Ice Cap, of slow and undifferentiated flow in the west and center and relatively fast-flowing outlet glaciers separated by slower-flowing ice, is linked to several factors: (1) the relatively smooth bed topography of the west side of the ice cap as compared to the more mountainous and much more dissected bedrock topography elsewhere (Figure 8) and (2) the relative lack of precipitation and hence mass turnover on the northwestern side of the ice cap [*Koerner*, 1979]. This flow pattern appears typical of many large (10^3 km^2) Arctic ice caps, which are also differentiated into fast- and slow-flowing elements, for example, Academy of Sciences Ice Cap, Severnaya Zemlya, and Austfonna, Svalbard [*Dowdeswell et al.*, 1999, 2002]. In addition, SAR interferometry of the Academy of Sciences Ice Cap also shows a region of undifferentiated flow in the precipitation shadow of the ice cap crest [*Dowdeswell et al.*, 2002].

[36] Fast-flowing features in the velocity structure of the Devon Ice Cap are usually associated with troughs in the bedrock beneath the ice (Figures 10a and 10b). This is consistent with the likely thermal structure of the ice cap, where basal melting will take place first beneath thick ice located in bedrock troughs [e.g., *MacAyeal*, 1993]. Analysis of the subglacial topography in regions near the onset of fast flow at the heads of outlet glaciers indicates that the transition from slow to fast glacier flow tends to occur in two different bedrock-topographic settings. The first type of transition zone is characterized by the presence of a bedrock step at the location where marked acceleration occurs. An example is provided by the two glaciers that drain from the southwest region of the ice cap into Croker Bay (Figure 10a). Ice flow from ~15 km up-glacier of the area where rapid flow begins is strongly convergent, and the ice surface slope increases from ~1° to ~7° over a bedrock step. These characteristics are similar to those of a number of outlet glaciers that drain the East Antarctic Ice Sheet [*McIntyre*, 1985], where a step in the subglacial topography is associated with the initiation of fast flow and also provides a "pinning point" that appears to restrict the propagation of fast flow farther inland.

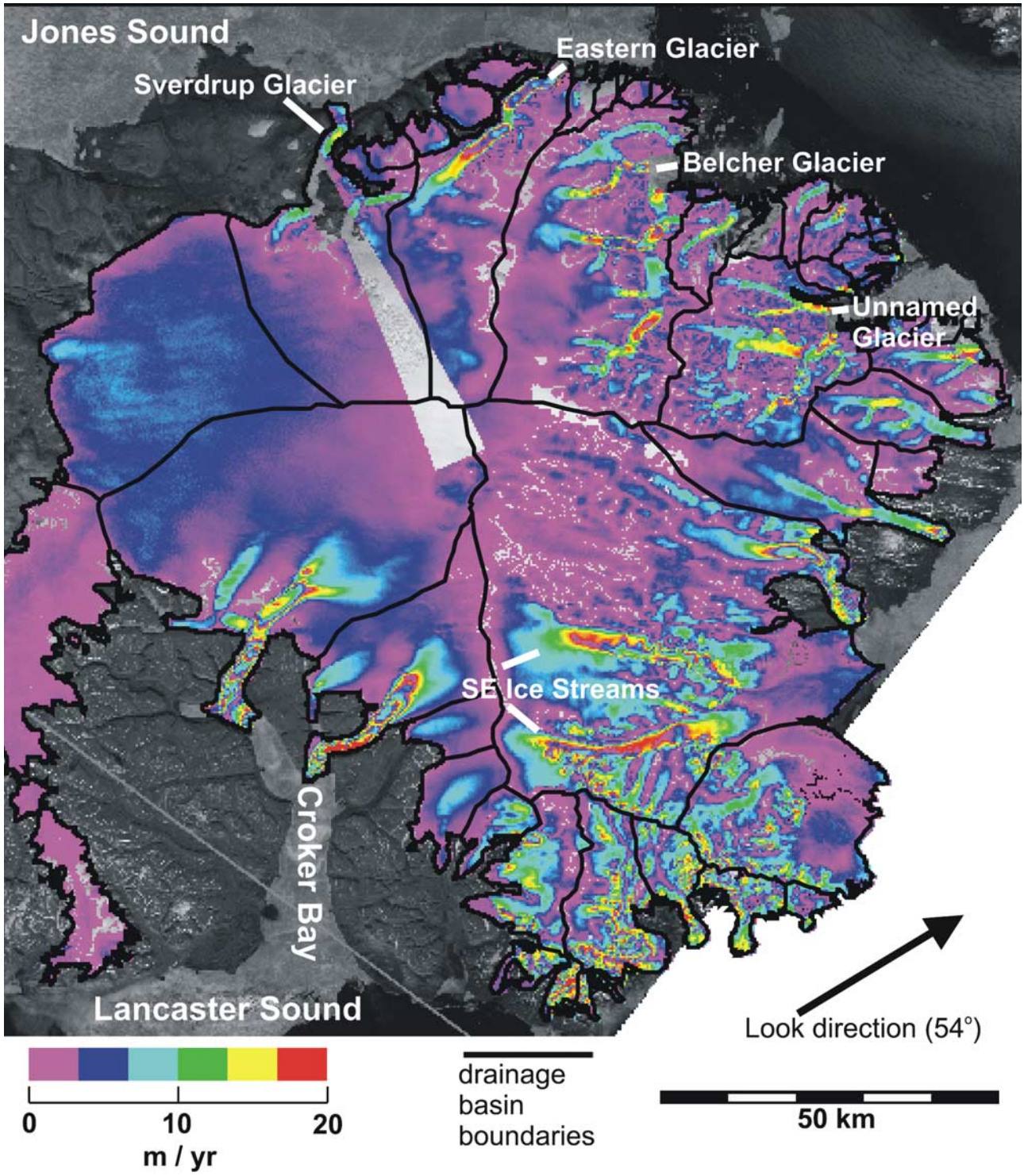

Figure 9. Synthetic aperture radar interferogram of the Devon Ice Cap. Ice surface velocities are given in the look direction of the satellite, which is indicated by an arrow. The interferometric fringes are overlaid on a 1999 Landsat 7 ETM+ image.

[37] A second type of transition between slow and fast glacier flow occurs at the head of most of the outlet glaciers that drain the eastern half of the Devon Ice Cap. Here ice flow is generally nonconvergent, surface slopes are consistently low (~1°), and surface velocities increase gradually down-glacier (Figure 9). The lack of distinct pinning points along these outlet glaciers suggests that there is no constraint on the up-glacier propagation of enhanced glacier flow. This may explain why the two well-developed fast-flow units in the southeast region of the ice cap currently extend inland almost to the main north-south ice divide (Figure 9). The velocities of these two fast-flowing glaciers also decrease significantly

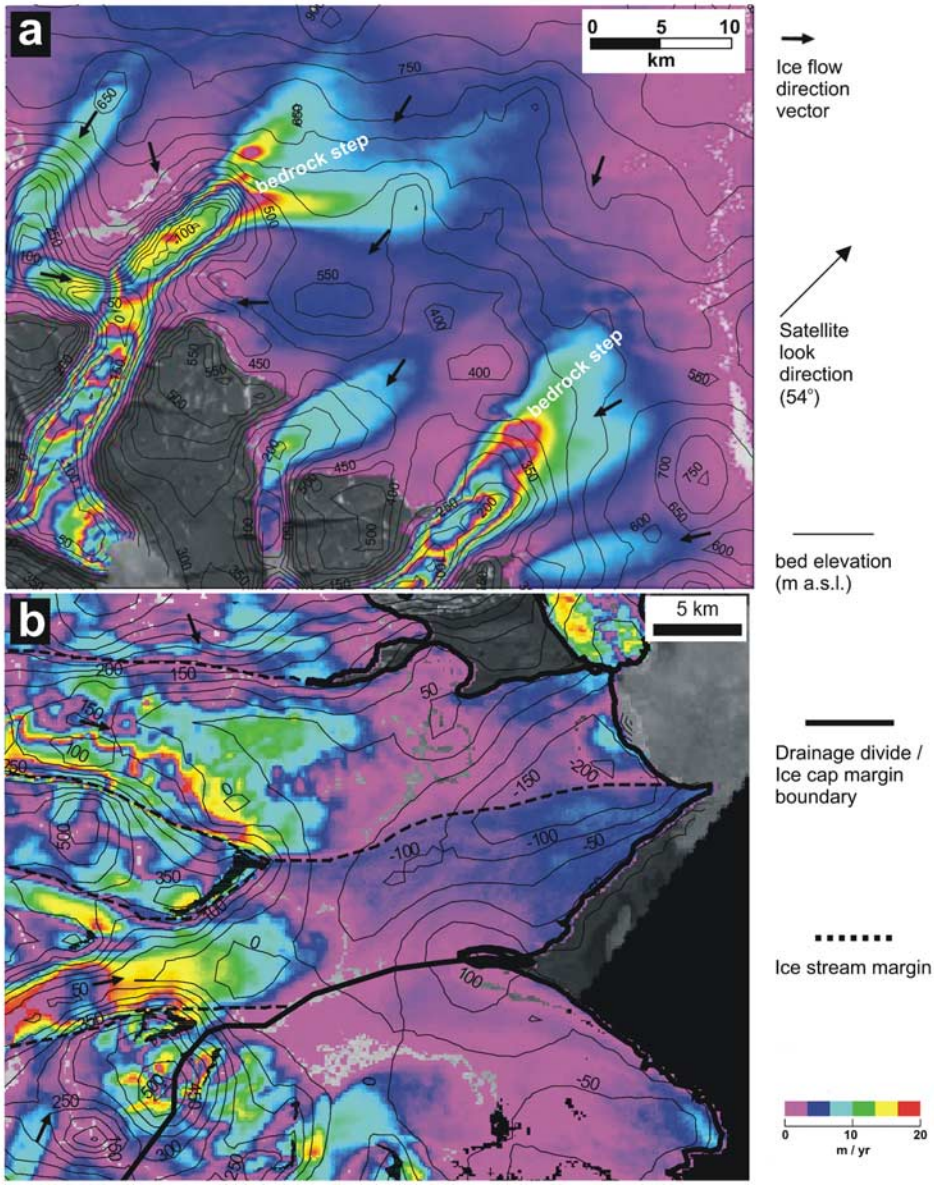

Figure 10. Ice surface velocity (in the satellite look direction) and subglacial bedrock topography (from radio echo data) for two parts of the Devon Ice Cap. (a) Two outlet glaciers draining southwest into Croker Bay. (b) Low-gradient piedmont lobe draining east from the Devon Ice Cap and fed by several outlet glaciers. The ice flow direction (inferred from the direction of maximum ice surface slope) is shown by arrows.

down-glacier of the point beyond which ice flow is no longer constrained laterally by bedrock structures and the ice streams are no longer fed by tributary ice flows (Figure 10b).

4.3. Driving Stresses From Radar-Derived Topographic Data

[38] The pattern of driving stresses (τ) on the Devon Ice Cap is calculated from the data on ice surface slope (α) and ice thickness (h) in our radar-derived digital elevation models (Figures 5 and 7). The driving stresses mapped in Figure 11 are calculated using the equation $\tau = \rho_i g h \sin\alpha$, where ρ_i is ice density and g is the acceleration due to gravity. The absolute values of calculated driving stress will vary with the amount of smoothing of the ice surface slopes [*Paterson*, 1994], but the spatial pattern of the stresses will remain unaltered.

[39] Driving stresses are generally lowest close to the ice divides on the Devon Ice Cap (Figures 3 and 11) and also on the piedmont lobes draining the southeast of the ice cap, where they reach <50 kPa. Although low in relative terms, the driving stresses in the piedmont lobe are significantly higher than those recorded in the ice streams of West Antarctica [e.g., *Cooper et al.*, 1983; *Bentley*, 1987].

5. Conclusions

[40] 1. Our airborne 100 MHz radar investigations of the morphology of the Devon Ice Cap acquired a total of 3370 km of radar data. The ice cap was covered by a nominal 10 km spaced grid of flight lines, with additional lines obtained from a number of outlet glaciers (Figure 3).

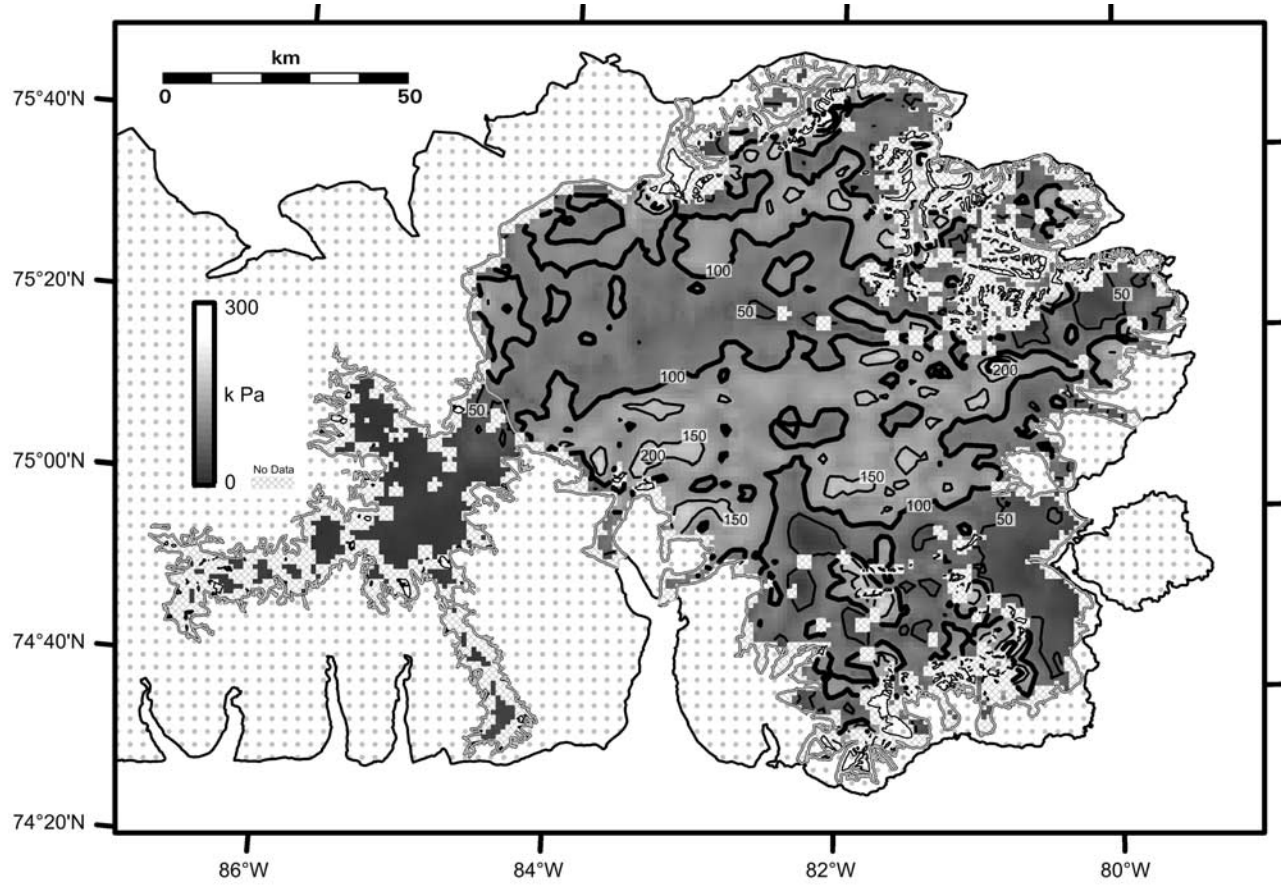

Figure 11. Distribution of driving stresses on the Devon Ice Cap (contour interval 50 kPa).

Radar returns from the ice cap bed were obtained from over 90% of flight tracks. Mean crossing point errors in ice surface elevation and ice thickness were 7–8 m.

[41] 2. Reduced radar measurements were interpolated over the whole ice cap to produce DEMs of ice cap surface and bed elevation, together with ice thickness. These DEMs can be used in numerical modeling studies of the ice cap. Until now, numerical modeling of Canadian Arctic ice caps, and thus predictions of their likely responses to future and past climate changes, has been largely precluded because very little information has been available on their three-dimensional morphology.

[42] 3. The total area of the Devon Ice Cap is 14,010 km^2, measured digitally from Landsat imagery (Figure 3). However, a 1960 km^2 ice-covered area extending westward from the main ice cap is stagnant and dynamically separate (Figure 4a). Subtracting this gives an area of 12,050 km^2 for the Devon Ice Cap proper. The largest drainage basin is 2630 km^2 in area (Figure 3).

[43] 4. The central area of the Devon Ice Cap is relatively simple and dome-like in shape (Figures 3 and 5). The ice cap crest has a maximum measured elevation of 1921 m. The area-elevation curve, important in mass balance studies, is relatively smooth, with a minor peak at ~1000–1100 m above sea level (Figure 6). The ice cap is drained by a number of outlet glaciers, usually constrained by valley walls and up to ~35 km long.

[44] 5. The total length of tidewater ice cliffs at the margins of the Devon Ice Cap is 73 km (~4% of the ice cap edge). Icebergs are produced from the crevassed tidewater margins of the ice cap. The largest icebergs observed on Landsat imagery and during airborne radar work were <100 m in maximum diameter (Figure 4c). There is little evidence that these tidewater ice margins are floating.

[45] 6. The maximum thickness of ice recorded on Devon Island is 880 m, just southeast of the center of the ice cap. An ice volume of 3980 km^3 is calculated, which is equivalent to ~10 mm of global sea level.

[46] 7. Only 8% of the ice cap bed lies below present sea level (Figure 6b). The bed is an upland plateau, dissected by a series of steep-sided valleys (Figure 8). The subglacial valleys and subaerial valley walls appear to control the locations of the major outlet glaciers draining the Devon Ice Cap.

[47] 8. Landsat imagery was used to examine the drainage basins and outlet glaciers of the Devon Ice Cap for indications of present or past surge activity. Only a single outlet glacier of the ice cap showed signs of past instability [*Copland et al.*, 2003]. However, all the major outlet glaciers along the eastern margin of the ice cap have experienced retreat, ranging from 1 to 3 km since 1960.

[48] 9. SAR interferometry was used to map the velocity structure of the Devon Ice Cap and, in particular, the extent and distribution of fast-flowing ice (Figure 9). Slow and undifferentiated flow predominates in the west and central region of the ice cap, with fast-flowing outlet glaciers and intervening slow-flowing ridges typical elsewhere (Figures 9 and 10). Outlet glacier velocities are

typically 7–10 times higher than in adjacent areas of undifferentiated flow.

[49] 10. Fast-flowing outlets usually occupy troughs in the bedrock topography (Figures 8 and 10), consistent with an ice cap thermal structure where basal melting is likely to take place first beneath thick ice located in bedrock troughs [e.g., *MacAyeal*, 1993]. This velocity structure, of fast-flowing units set within slower-flowing ice, appears typical of many large Arctic ice caps as well as of the great ice sheets of Antarctica and Greenland.

[50] **Acknowledgments.** This study was funded by the NERC Centre for Polar Observation and Modelling, UK, by NERC grant GR3/12469, and by the EU SPICE Project to J.A.D. as well as by grants from the Meteorological Service of Canada (CRYSYS program) to M.J.S. D.B. acknowledges receipt of an NSERC IPS scholarship. We thank Kenn Borek Aviation for air support and the Polar Continental Shelf Project (PCSP), Canada, for ground support at Resolute Bay. The paper is PCSP contribution 02003. We are grateful to R. M. Koerner, who provided advice and support throughout the project and who read the manuscript. Robin Bassford assisted with the field program. Liz Morris kindly assisted with data and support for GPS differential postprocessing. Waleed Abdalati, Douglas Mair, and Liz Morris provided surface elevation points.

References

Andrews, J. T. (2002), Glaciers of Canada: Glaciers of Baffin Island, *U.S. Geol. Surv. Prof. Pap.*, *1386-J*, 165–198.

Benham, T. J., and J. A. Dowdeswell (2003), A simple visualisation method for distinguishing between subglacial-bed and side-wall returns in radio-echo records from outlet and valley glaciers, *J. Glaciol.*, *49*, 463–468.

Bentley, C. R. (1987), Antarctic ice streams: A review, *J. Geophys. Res.*, *92*, 8843–8858.

Bindschadler, R., J. A. Dowdeswell, D. Hall, and J.-G. Winther (2001), Glaciological applications with Landsat-7: Early assessments, *Remote Sens. Environ.*, *78*, 163–179.

Cattle, H., and J. Crossley (1995), Modelling Arctic climate change, *Philos. Trans. R. Soc. London, Ser. A*, *352*, 201–213.

Cooper, A. P. R. (1987), Interface tracking in digitally recorded glaciological data, *Ann. Glaciol.*, *9*, 50–54.

Cooper, A. P. R., N. F. McIntyre, and G. de Q. Robin (1983), Driving stresses in the Antarctic ice sheet, *Ann. Glaciol.*, *3*, 59–64.

Copland, L., M. Sharp, and J. A. Dowdeswell (2003), The distribution and flow characteristics of surge-type glaciers in the Canadian High Arctic, *Ann. Glaciol.*, *36*, 73–81.

Cress, P., and R. Wyness (1961), The Devon Island expedition: Observations of glacial movement, *Arctic*, *14*, 257–259.

Doake, C. S. M., M. Gorman, and W. S. B. Paterson (1976), A further comparison of glacier velocities measured by radio-echo and survey methods, *J. Glaciol.*, *17*, 35–38.

Dowdeswell, J. A. (1995), Glaciers in the High Arctic and recent environmental change, *Philos. Trans. R. Soc. London, Ser. A*, *352*, 321–334.

Dowdeswell, J. A., and J. O. Hagen (2004), Arctic glaciers and ice caps, in *Mass Balance of the Cryosphere*, edited by J. L. Bamber and A. J. Payne, pp. 527–557, Cambridge Univ. Press, New York.

Dowdeswell, J. A., and M. Williams (1997), Surge-type glaciers in the Russian High Arctic identified from digital satellite imagery, *J. Glaciol.*, *43*, 489–494.

Dowdeswell, J. A., M. R. Gorman, A. F. Glazovsky, and Y. Y. Macheret (1994), Evidence for floating ice shelves in Franz Josef Land, Russian High Arctic, *Arct. Alp. Res.*, *26*, 86–92.

Dowdeswell, J. A., A. F. Glazovsky, and Y. Y. Macheret (1995), Ice divides and drainage basins on the ice caps of Franz Josef Land, Russian High Arctic, defined from Landsat, Russian KFA-1000 and ERS-1 SAR satellite imagery, *Arct. Alp. Res.*, *27*, 264–270.

Dowdeswell, J. A., et al. (1997), The mass balance of circum-Arctic glaciers and recent climate change, *Quat. Res.*, *48*, 1–14.

Dowdeswell, J. A., B. Unwin, A.-M. Nuttall, and D. J. Wingham (1999), Velocity structure, flow instability and mass flux on a large Arctic ice cap from satellite radar interferometry, *Earth Planet. Sci. Lett.*, *167*, 131–140.

Dowdeswell, J. A., et al. (2002), Form and flow of the Academy of Sciences Ice Cap, Severnaya Zemlya, Russian High Arctic, *J. Geophys. Res.*, *107*(B4), 2076, doi:10.1029/2000JB000129.

Dyurgerov, M. B., and M. F. Meier (1997a), Year-to-year fluctuations of global mass balance of small glaciers and their contribution to sea-level change, *Arct. Alp. Res.*, *29*, 392–402.

Dyurgerov, M. B., and M. F. Meier (1997b), Mass balance of mountain and subpolar glaciers: A new global assessment for 1961–1990, *Arct. Alp. Res.*, *29*, 379–391.

Fisher, D. A., et al. (1998), Penny Ice Cap cores, Baffin Island, Canada, and the Wisconsinan Foxe Dome connection: Two states of Hudson Bay ice cover, *Science*, *279*, 692–695.

Gabriel, A. K., R. M. Goldstein, and H. A. Zebker (1989), Mapping small elevation changes over large areas: Differential radar interferometry, *J. Geophys. Res.*, *94*, 9183–9191.

Hagen, J. O., and N. Reeh (2004), Mass balance measurements, in *Mass Balance of the Cryosphere*, edited by J. L. Bamber and A. J. Payne, pp. 11–42, Cambridge Univ. Press, New York.

Higgins, A. K. (1991), North Greenland glacier velocities and calf ice production, *Polarforschung*, *60*, 1–23.

Hodgkins, R., and J. A. Dowdeswell (1994), Tectonic processes in Svalbard tidewater glacier surges: Evidence from structural glaciology, *J. Glaciol.*, *40*, 553–560.

Hutchinson, M. F. (1993), Development of a continent-wide DEM with applications for terrain and climate analysis, in *Environmental Modelling With GIS*, edited by M. F. Goodchild et al., pp. 392–399, Oxford Univ. Press, New York.

Isaaks, E. H., and R. M. Srivastava (1989), *Applied Geostatistics*, Oxford Univ. Press, New York.

Joughin, I., S. Tulaczyk, M. Fahnestock, and R. Kwok (1996), A mini-surge on the Ryder Glacier, Greenland, observed by satellite radar interferometry, *Science*, *274*, 228–230.

Koerner, R. M. (1977a), Devon Island Ice Cap—Core stratigraphy and paleoclimate, *Science*, *196*, 15–18.

Koerner, R. M. (1977b), Ice thickness measurements and their implications with respect to past and present ice volumes in the Canadian High Arctic ice caps, *Can. J. Earth Sci.*, *14*, 2697–2705.

Koerner, R. M. (1979), Accumulation, ablation and oxygen isotope variations in the Queen Elizabeth Island ice caps, Canada, *J. Glaciol.*, *22*, 25–41.

Koerner, R. M. (1997), Some comments on climatic reconstructions from ice cores drilled in areas of high melt, *J. Glaciol.*, *43*, 90–97.

Koerner, R. M. (2002), Glaciers of Canada: Glaciers of the High Arctic islands, *U.S. Geol. Surv. Prof. Pap.*, *1386-J*, 111–146.

Koerner, R. M., and D. A. Fisher (1990), A record of Holocene summer climate from a Canadian High-Arctic ice core, *Nature*, *343*, 630–631.

Lamoureux, S. F., R. Gilbert, and T. Lewis (2002), Lacustrine sedimentary environments in High Arctic proglacial Bear Lake, Devon Island, Nunavut, Canada, *Arct. Antarct. Alp. Res.*, *34*, 130–141.

Lythe, M. B., D. G. Vaughan, and BEDMAP Consortium (2001), BEDMAP: A new ice thickness and subglacial topographic model of Antarctica, *J. Geophys. Res.*, *106*, 11,335–11,352.

MacAyeal, D. R. (1993), Binge/purge oscillations of the Laurentide Ice Sheet as a cause of the North Atlantic's Heinrich events, *Paleoceanography*, *8*, 775–784.

Martin, P. J., and T. J. O. Sanderson (1980), Morphology and dynamics of ice rises, *J. Glaciol.*, *25*, 33–45.

Massonnet, D., M. Rossi, C. Carmona, F. Adragna, G. Peltzer, K. Feigl, and T. Rabaute (1993), The displacement field of the Landers earthquake mapped by radar interferometry, *Nature*, *364*, 138–142.

McIntyre, N. F. (1985), The dynamics of ice-sheet outlets, *J. Glaciol.*, *31*, 99–107.

Meier, M. F., and A. S. Post (1969), What are glacier surges?, *Can. J. Earth Sci.*, *6*, 807–817.

Paterson, W. S. B. (1994), *The Physics of Glaciers*, 3rd ed., Pergamon, New York.

Smith, B. M. E., and S. Evans (1972), Radio echo sounding: Absorption and scattering by water inclusions and ice lenses, *J. Glaciol.*, *11*, 133–146.

Williams, M., and J. A. Dowdeswell (2001), Historical fluctuations of the Matusevich Ice Shelf, Severnaya Zemlya, Russian High Arctic, *Arct. Antarct. Alp. Res.*, *33*, 211–222.

Zebker, H. A., C. L. Werner, P. A. Rosen, and S. Hensley (1994), Accuracy of topographic maps derived from ERS-1 interferometric radar, *IEEE Trans. Geosci. Remote Sens.*, *32*, 823–836.

T. J. Benham, J. A. Dowdeswell, and M. R. Gorman, Scott Polar Research Institute, University of Cambridge, Lensfield Road, Cambridge CB2 1ER, UK. (tjb52@cam.ac.uk; jd16@cam.ac.uk)

D. Burgess and M. J. Sharp, Department of Earth and Atmospheric Sciences, University of Alberta, Edmonton, Alberta, Canada T6G 2E3. (dob@ualberta.ca; martin.sharp@ualberta.ca)